Supplement of Atmos. Meas. Tech., 17, 1463–1474, 2024
https://doi.org/10.5194/amt-17-1463-2024-supplement

Atmospheric Measurement Techniques
Open Access
EGU

Supplement of

Performance characterization of a laminar gas inlet

Da Yang et al.

Correspondence to: Da Yang (da.yang@colorado.edu) and Suresh Dhaniyala (sdhaniya@clarkson.edu)

To understand the relation between turbulence in the freestream and that in the inner shroud, simulations for the freestream velocities of 75 to 180 m s^{-1} were repeated for freestream turbulent intensities ranging from 0.5 % to 3%. The range of turbulent intensities is determined by observing velocity fluctuations in the wind tunnel, recorded every 10 seconds from a Pitot tube inside the tunnel. The simulations were conducted under ground conditions listed in Table 1. The turbulent intensities (TI) obtained in the inner shroud at a selected location H (see Fig. 1) just upstream of the sampling tube entrance are shown in Figure S1.

The CFD results show that the turbulent intensity at location H increased with increasing freestream velocity and freestream turbulence. For all cases studied, turbulent intensity at location H calculated from the k-ε model was nearly twice that predicted by the SST model.

The outer shroud is used not only to decrease the flow velocity but also to ensure that the sample flow is insensitive to the aircraft's angle of attack. We simulated the performance of the inlet with 25mm restrictor for 3° and 20° angle of attack for 4 different freestream velocities corresponding to wind-tunnel experimental conditions. As shown in Figure S2, less than 5% difference in flow velocities at different locations within the shroud for all simulation cases. The CFD results suggest that the shroud ensures sampling performance that is independent of angle of attack.

Our simulations tested a wide range of sampling flow velocity from laminar flow to turbulent flow at both ground level and high-altitude conditions. As shown in Figure S3, overall gas sampling efficiency is highly correlated with local sampling flow rate across two distinct altitudes. The k-ε model predict more loss (10%~20%) than SST model due the higher predictions of turbulent diffusivity. In addition, the results show ~20% higher sampling efficiency using H_2SO_4 laminar diffusivity under laminar or near-laminar sampling flow conditions.

We observed turbulent diffusivity dissipating further along the sampling tube, especially in cases with low Reynolds Numbers in the sampling tube. As illustrated in Figure S4, where the Reynolds Number is ~700, laminar diffusivity can significantly contribute to the diffusion coefficient near the sampling outlet.

Furthermore, we investigated different boundary conditions for the mass fraction of water at the wall. Figure S5 illustrates a linear relationship between overall gas sampling efficiency at the sampling outlet and the mass fraction at the wall under the same operating condition. Thus, as the walls soak up the depositing gas-species, the loss to walls with reduce and eventually desorption of the gas is possible.

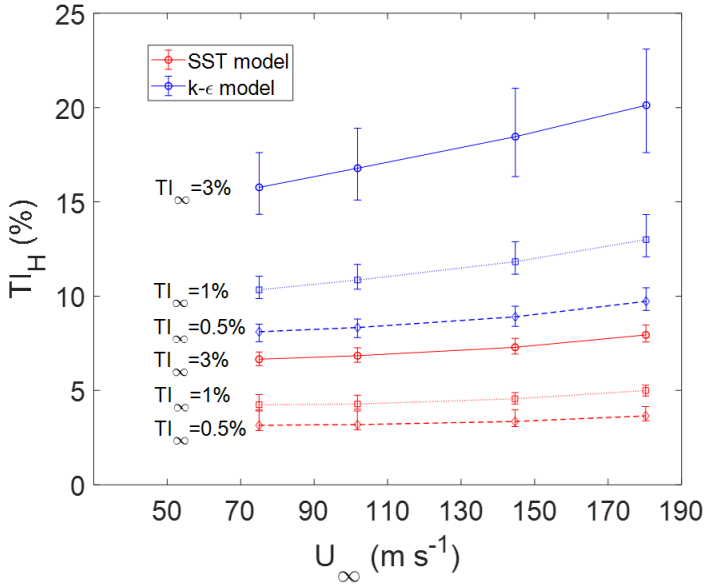

Figure S1: Comparisons of turbulent intensities obtained with k-ε and SST models at ground-level. Turbulent intensity is reported at location H in the inner shroud, corresponding to the location where a hotwire probe is located. The uncertainty bar in this plot represents the range of intensity for a 0.5*1cm^2 area at this location.

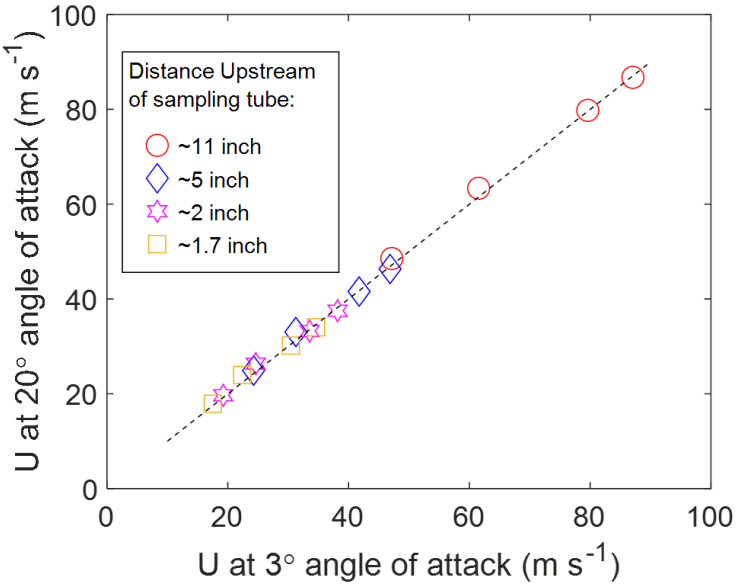

Figure S2: Comparisons for flow velocities (U) at different locations within the shroud, for two angles of attack: 3° and 20° and range of freestream velocities. The modelling conditions were freestream pressure of 97,000 Pa, restrictor size 25mm and sample velocity of 2.4 m s^{-1} (Table 1)

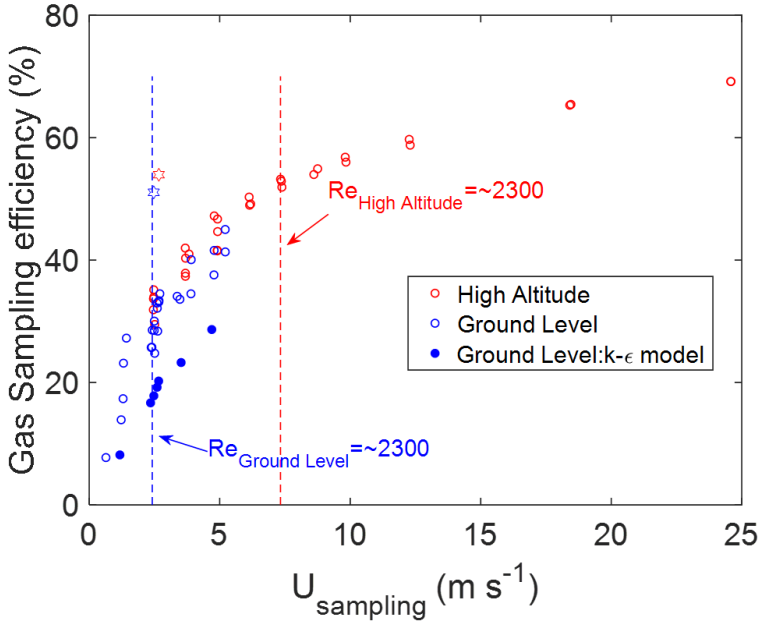

Figure S3: Comparisons for overall gas sampling efficiency under different sampling flow velocities ($U_{sampling}$) at different altitudes. The hollow points show the results from SST model from two altitudes and solid points show the prediction from k-ε model at ground level. The dash lines marked sampling flow reach the Reynolds number of 2300 in our half-inch sampling tube at different altitudes respectively. Two hollow hexagram points present two cases using diffusivity of H_2SO_4 instead of water vapor.

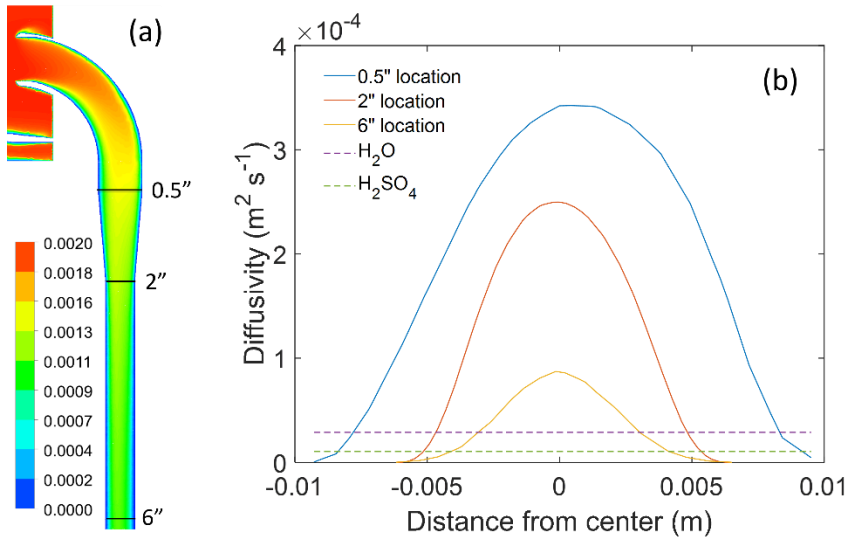

Figure S4: Simulation results at high altitude conditions in Table 1 (220 m s^{-1}, 12.5mm restrictor, sample velocity of 2.4 m s^{-1}). (a) The contour of mass fraction in the center plane of the sampling tube, with different locations relevant for (b). (b) Diffusivity distribution along each line across the center plane marked in (a). Solid lines represent turbulent diffusivity distribution at different locations, dash lines represent the constant laminar diffusivity of two different gas phase species as references.

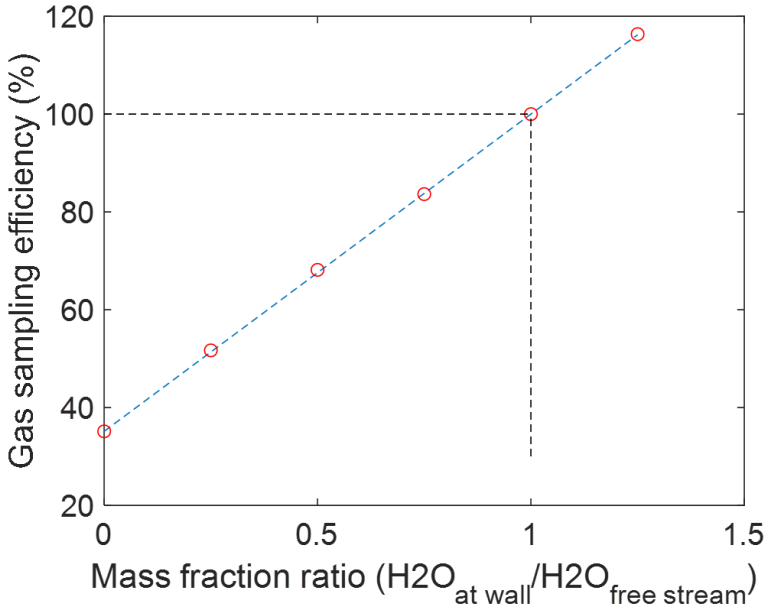

Figure S5: Overall gas sampling efficiency for high altitude conditions in Table 1 (220 m s^{-1}, 12.5mm restrictor, sample velocity of 2.4 m s^{-1}) under different boundary conditions set for mass fraction of water vapor at the wall.